

Quantum information processing and cavity QED experiments with trapped Ca^+ ions

S. Gulde, H. Häffner, M. Riebe, G. Lancaster, A. Mundt, A. Kreuter, C. Russo, C. Becher, J. Eschner, F. Schmidt-Kaler, I. L. Chuang[†], and R. Blatt

*Institut für Experimentalphysik, Universität Innsbruck,
Technikerstrasse 25, A-6020 Innsbruck, Austria*

Abstract

Single trapped Ca^+ ions, stored in a linear Paul trap and laser-cooled to the ground state of their harmonic quantum motion are used for quantum information processing. As a demonstration, composite laser pulse sequences were used to implement phase gate and CNOT gate operation. For this, Stark shifts on the qubit transitions were precisely measured and compensated. With a single ion stored inside a high-finesse optical cavity, a cavity mode can be coherently coupled to the qubit transition.

1 Quantum information processing

1.1 Experimental setup

Trapped and laser cooled atoms are a promising and potentially scalable approach to quantum computation [1]. While long-lived internal states hold the quantum information, the quantized common motion in the confining trap is used to create entanglement and for quantum information processing. As shown in Fig. 1, with single trapped Ca^+ ions we realize the quantum bit (qubit) by operating on a narrow optical S–D (quadrupole) transition. The S \leftrightarrow P \leftrightarrow D dipole transitions are driven for optical cooling, state preparation, and state detection.

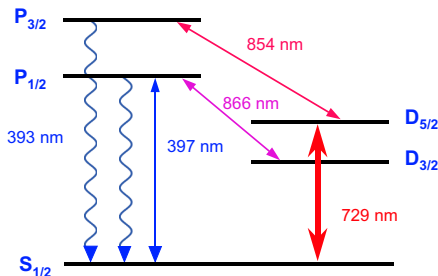


Figure 1: Ca^+ level scheme. The narrow quadrupole transition ($\tau_D = 1$ s) at 729 nm serves to implement the qubit. Lasers at 397 nm and 866 nm are used for the excitation of resonance fluorescence and for Doppler cooling, the laser at 854 nm is used for repumping. The laser system is described in detail elsewhere [2].

For quantum information processing we load ions into a linear Paul trap with axial (radial) frequency $\nu_z \simeq 1.7$ MHz ($\nu_r \simeq 5$ MHz). Doppler cooling [3] is achieved by tuning the 397 nm laser below the resonance while keeping the 866 nm laser near resonance to prevent shelving in the $D_{3/2}$ level. Within 2 ms, a single ion (or a string of ions) is cooled to residual vibrational excitation numbers of about $\bar{n}_z \simeq 20$ in the axial direction and $\bar{n}_r \simeq 3$ in the radial direction. Further cooling to the ground state of the axial motion is achieved by sideband cooling [4]. We strongly saturate

the $S_{1/2}(m = 1/2) \leftrightarrow D_{5/2}(m = 5/2)$ transition on the lower axial sideband, i.e. with a detuning of the 729 nm laser $\Delta = -\nu_z$, while shining in laser light at the 854 nm transition to quench the $D_{5/2}$ state population via the $P_{3/2}$ state. Optical pumping to the $S_{1/2}(m = -1/2)$ level is prevented by occasional short laser pulses of σ^+ polarized light at 397 nm. The ground state occupation is found by comparison of the on-resonance excitation probability for red and blue sideband transitions and is routinely $> 99\%$ for a single ion after about 10 ms of cooling [4].

With ion strings of up to three ions, individual addressing of an arbitrary ion in the string is routinely achieved by steering the 729 nm beam with an electro-optic deflector [5]. The addressing resolution is $2.8(1) \mu\text{m}$. For a three-ion string, the laser intensity on a neighboring ion is 1% of the intensity on the addressed ion.

1.2 Qubit manipulation

Quantum information processing requires that individual qubits can be coherently manipulated. Together with a 2-qubit controlled-NOT operation this provides a set of universal gate operations, i.e. arbitrary quantum computations can then be performed using sequences of these gate operations. Thus, the capability to perform these one and two-qubit rotations is at the heart of quantum information processing. We realize single-qubit rotations by coherent manipulation of the $S_{1/2}(m = 1/2) \leftrightarrow D_{5/2}(m = 1/2)$ transition in Ca^+ . Coupling two qubits requires the precise control of the motional state of a single ion or a string of ions [1]. Both operations can be performed by applying laser pulses at the carrier (no change of vibrational quantum number, $\Delta n_z = 0$) or one of the sidebands (laser detuned by $\pm\nu_z$, $\Delta n_z = \pm 1$) of the S–D transition as indicated in Fig. 2.

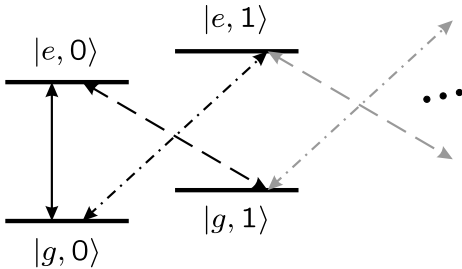


Figure 2: Lowest levels of a single trapped ion. The internal levels $|g\rangle, |e\rangle$ correspond to the $S_{1/2}(m = 1/2)$, $D_{5/2}(m = 1/2)$ states, respectively, and the numbers $n = 0, 1$ denote the quantum number of the axial motion.

Qubit rotations can be written as unitary operations in the following way [6]: Carrier rotations (*i.e.* $|g, n\rangle \leftrightarrow |e, n\rangle$ transitions) are given by

$$R(\theta, \phi) = \exp\left[i\frac{\theta}{2}(e^{i\phi}\sigma^+ + e^{-i\phi}\sigma^-)\right], \quad (1)$$

whereas transitions on the upper (blue or +) and lower (red or -) sidebands are denoted as

$$R^+(\theta, \phi) = \exp\left[i\frac{\theta}{2}(e^{i\phi}\sigma^+ a^\dagger + e^{-i\phi}\sigma^- a)\right] \quad (2)$$

$$R^-(\theta, \phi) = \exp\left[i\frac{\theta}{2}(e^{i\phi}\sigma^+ a + e^{-i\phi}\sigma^- a^\dagger)\right], \quad (3)$$

where $\sigma^\pm = (\sigma_x \pm i\sigma_y)$ act on the internal state of the ion (notation: $\sigma^+ = |e\rangle\langle g|$) and a, a^\dagger account for the harmonic oscillation (*i.e.* the annihilation or creation of a

phonon at the trap frequency). The parameter θ depends on the strength and the duration of the applied pulse and ϕ is its phase, *i.e.* the relative phase between the optical field and the atomic polarization. Fig. 3 shows an example of coherent Rabi oscillations for an excitation on the carrier and the blue sideband, respectively. A

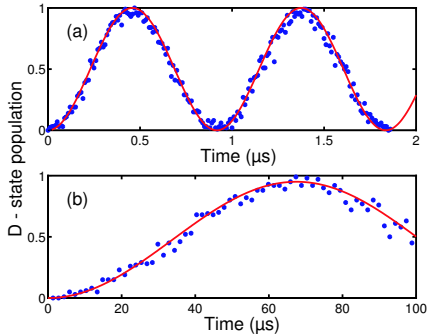


Figure 3: Rabi oscillations on (a) the carrier and (b) the blue sideband. Note that the time scale is different for (a) and (b). The blue sideband coupling is reduced by the Lamb–Dicke factor $\eta = ka_0$ (typically on the order of 10^{-2} for Ca^+), where k is the wavenumber of the 729 nm radiation and a_0 denotes the size of the ground state wavefunction.

quantum algorithm is implemented by concatenating pulses on the carrier and on the sidebands. Since already the simplest algorithms require several pulses, it is imperative to control precisely the relative optical phases of these pulses or, at least, to keep track of them such that the required pulse sequences lead to the desired operations. In particular, this requires the precise consideration of all phases introduced by the light shifts of the exciting laser beams.

1.3 Stark shift measurements and compensation

As can be inferred from the level scheme (cf. Fig. 1) ac–Stark shifts do appear in this system since the manipulating laser beam at 729 nm acts off-resonantly on the various Zeeman components of the $S \leftrightarrow D$ transitions and their motional sidebands, as well as on the other $S \leftrightarrow P$ and $D \leftrightarrow P$ dipole transitions. The individual shifts have different signs and compensate each other only to some extent. However, since the detuning and the interaction time of the 729 nm laser changes depending on the pulse sequence pertaining to an algorithm, these combined shifts (which are typically of the order of several kHz) can not be neglected and must be carefully controlled.

For a precise measurement of the Stark shift we used a Ramsey type interference experiment. Fig. 4 shows the measurement procedure and the result. We first apply a $\pi/2$ -pulse on the carrier, then apply a pulse of variable length at a specific detuning, and eventually close the Ramsey-cycle with another $\pi/2$ -pulse. Thus, if there is no phase shift, the population is transferred to the excited state, whereas in the presence of light-shifts the phase of the transition is affected and accordingly results in the observed Ramsey fringes of the D-state population. The frequency of the observed sinusoidal variation is a direct measure of the light shift.

Fig. 5 shows the measured light shifts for various detunings around the qubit transition. Note that for detunings larger than ~ 6 MHz the combined phase shift changes sign. A positive net shift is also observable for detunings below the qubit resonance.

The precise knowledge of magnitude and sign of the light shift allows for compensating the unwanted Stark shift created by a gate pulse by applying an additional off-resonant pulse simultaneously. For example, for an excitation on the blue sideband

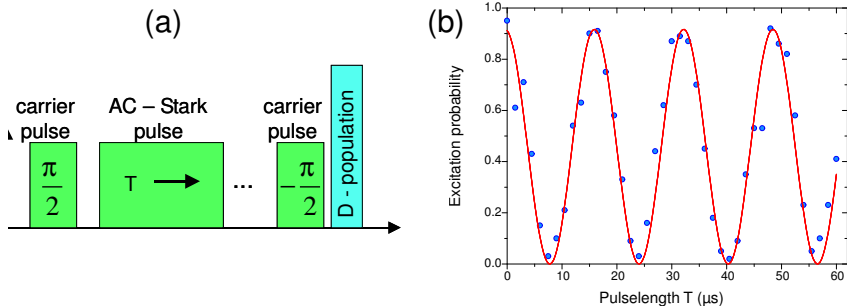


Figure 4: (a) Ramsey technique to measure light shifts, see text. (b) Observed Ramsey fringes as a function of the applied pulse length. The frequency of the sinusoidally varying signal corresponds to the light shift.

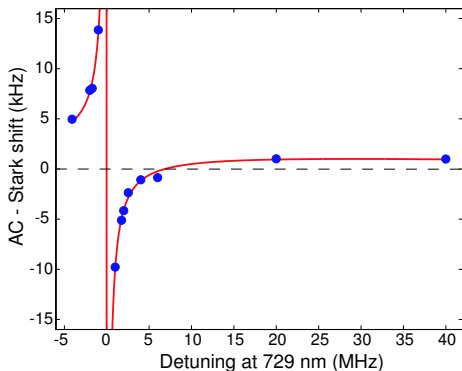


Figure 5: Light shift in the vicinity of the qubit transition.

($\nu_z \simeq 1.7$ MHz) the net Stark shift is negative, thus the simultaneous application of an additional off-resonant pulse which leads to the same positive shift should be able to compensate the shift of the gate pulses. We implemented this procedure experimentally and showed by measurements as in Fig. 4 that light shifts can indeed be reduced to below 2% of the value without compensation. Using this compensation technique, arbitrary pulse sequences can be concatenated without the necessity to keep track of the changing phase.

1.4 Composite quantum operations with ions

Aside from controlling the optical phases, quantum information processing with ions requires also the precise control of the quantum state of *motion*. In particular, for operations which encode one qubit in the $|n\rangle = |0\rangle, |1\rangle$ motional states (such as the Cirac-Zoller CNOT operation [1]) it is important that after each gate operation no population has leaked from the computational subspace $|g, 0\rangle, |e, 0\rangle, |g, 1\rangle, |e, 1\rangle$. If that were not the case, any series of operations would eventually lose its fidelity and it would not be possible to work through an extended algorithm. The major problem here is that due to the degenerate harmonic oscillator structure of the level scheme, sideband pulses (red and blue) work simultaneously on all levels. Therefore any population in $|e, 1\rangle$ (or $|g, 1\rangle$) prior to a red (or blue) sideband pulse will leave

the computational subspace. In order to avoid this, one can use composite pulses, *i.e.* a sequence of carrier and/or sideband pulses instead of a single pulse. This method is well known in NMR technology and was recently proposed for application with trapped ions [6, 7].

For example, starting with a population in the $|e, 0\rangle$ state only, the application of a red sideband pulse with $\theta = \pi$ (a π -pulse) would correspond to a simple SWAP operation, and the population after the pulse would be $|g, 1\rangle$ only. However, this holds only if there was no population in the $|e, 1\rangle$ state initially. A composite SWAP pulse sequence such as

$$R_{\text{SWAP}} = R^-(\pi/\sqrt{2}, 0) R^-(2\pi/\sqrt{2}, \phi_{\text{SWAP}}) R^-(\pi/\sqrt{2}, 0) \quad (4)$$

where

$$\phi_{\text{SWAP}} = \cos^{-1}(\cot^2(\pi/\sqrt{2})) \approx 0.303 \pi \quad (5)$$

performs a perfect SWAP operation (*i.e.* a π -pulse) on the $|e, 0\rangle \leftrightarrow |g, 1\rangle$ transition and simultaneously does a 4π rotation on the $|e, 1\rangle \leftrightarrow |g, 2\rangle$ transition [8]. Similarly, more complicated operations, as e.g. a phase gate operation can be implemented in the same way [6, 8].

As an example, we demonstrate here a composite phase gate operation with a single ion which is implemented by the pulse sequence

$$R_{\text{phase gate}} = R^+(\pi, \pi/2) R^+(\pi/\sqrt{2}, 0) R^+(\pi, \pi/2) R^+(\pi/\sqrt{2}, 0). \quad (6)$$

This phase gate flips the sign of the states $|g, 0\rangle$, $|g, 1\rangle$, and $|e, 1\rangle$, but leaves the state $|e, 0\rangle$ unchanged. We implemented the procedure experimentally and measured the sign change by sandwiching the pulse sequence of Eq. (6) between two Ramsey carrier pulses as shown in Fig. 6. The initial state for the phase gate, as prepared by the first $\pi/2$ Ramsey pulse, is $(|g, 0\rangle + |e, 0\rangle)/\sqrt{2}$, which is transformed into $(-|g, 0\rangle + |e, 0\rangle)/\sqrt{2}$. Due to the opposite sign change of $|g, 0\rangle$ and $|e, 0\rangle$, the final $-\pi/2$ Ramsey pulse leads into $|e, 0\rangle$ with 97.8(5)% probability, rather than back into $|g, 0\rangle$.

Note that the total pulse sequence including the Ramsey pulses can also be read as a "zero-controlled NOT" operation, *i.e.* the internal state flips if and only if the motional state is $|n\rangle = |0\rangle$.

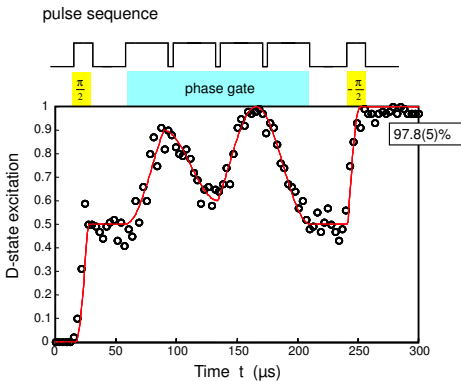


Figure 6: Verification of the composite phase gate with a single trapped ion. Circles show the excited state population when the pulse sequence is interrupted at time t . The solid line displays the calculated time evolution for an ideal pulse sequence as in Eq. (6).

We would like to point out that composite pulses eliminate the need for auxiliary levels to implement gate operations. For example, the Cirac-Zoller type CNOT gate [1] may be realized with an atomic 2-level system using composite pulses.

2 Cavity QED with single ions

2.1 Setup and measurement procedure

Quantum information processing with trapped ions is a scalable technology in principle. In practice, scaling current experiments to very long strings of ions is a very difficult task. However, since small scale quantum computers with up to about ten ions (maybe even a few ten ions) seem not unrealistic at present, it is a worthy effort to think and work about the technology to interconnect small ion trap quantum computers. Such a technique has been proposed by Cirac et al. [9] who considered a single trapped ion (as the qubit) inside a high-finesse cavity. Using a well-defined pulse shaping procedure, they show how a static qubit (e.g. encoded in the S–D states of Ca^+) can be converted to a "flying" qubit, i.e. a photon which is coupled through a photonic channel and which can be subsequently rewritten to another ion coupled again to a high-finesse optical cavity.

In order to investigate the first steps of such a device, we studied the coupling of the S–D qubit to the mode of a high-finesse cavity [11]. The setup of this experiment is schematically shown in Fig. 7. The single Ca^+ ion in the 3-dimensional RF-Paul trap has secular frequencies $\omega_{x,y,z} = 2\pi \times (2.9, 3.9, 7.4)$ MHz. The trap is placed in the center of a near-confocal resonator with mirror separation $L = 21$ mm, radius of curvature $R_M = 25$ mm, waist radius $\omega_0 = 54 \mu\text{m}$, and finesse $\mathcal{F} = 35000$ at 729 nm. Cylindrical piezoceramics (PZT) allow fine-tuning of the cavity length across approx. 1.5 free spectral ranges.

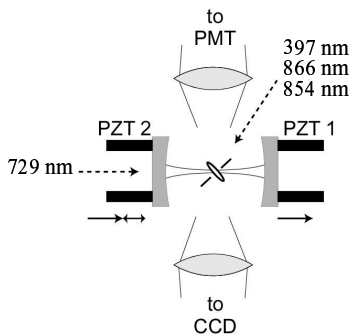


Figure 7: Schematic experimental setup. PZT1 denotes the offset piezo, PZT2 the scan piezo (see text). A photomultiplier (PMT) records fluorescence on the $S_{1/2} - P_{1/2}$ transition and the CCD camera monitors the ion's position. The dotted arrows indicate directions of laser beams.

Coherent coupling of the ion to the cavity field is measured in three steps:

(i) *Preparation*: First we apply Doppler cooling on the $S_{1/2} - P_{1/2}$ transition at 397 nm (see Fig. 7). From the measured mean vibrational quantum numbers after Doppler cooling, $(\bar{n}_x, \bar{n}_y, \bar{n}_z) = (20 \pm 5, 4 \pm 1, 6 \pm 1)$, we calculate an rms extension of the ion's motional wave packet of 25 ± 5 nm along the cavity axis, much smaller than the wavelength of 729 nm (Lamb-Dicke regime). After cooling, the ion is prepared in the $S_{1/2}(m = -1/2)$ substate by optical pumping with σ^- radiation at 397 nm.

(ii) *Interaction*: The laser at 729 nm is set to a fixed detuning Δ from the $S_{1/2} - D_{5/2}$ ($m = -1/2$ to $m' = -5/2$) qubit transition. We inject the laser light into the TEM₀₀ mode of the cavity and scan the cavity with a voltage ramp applied to the scan PZT (PZT2). When the cavity reaches resonance with the laser frequency, it fills with light and the ion is excited. The scan rates used are such that the cavity is swept over its HWHM bandwidth ($2\pi \times 0.10$ MHz) in 1.5...6 cavity lifetimes of 0.78 μs .

(iii) *State analysis*: Resonant excitation on the $S_{1/2} - P_{1/2}$ dipole transition at 397 nm is used to discriminate between excited state (electron shelved in $D_{5/2}$, no fluorescence) and ground state (fluorescence). A short pulse of 854 nm light returns the ion to the ground state if it was found in the $D_{5/2}$ state. Note that although state detection happens about 1 ms after the cavity-ion interaction, the ion's state is well preserved due to the long lifetime (1 s) of the $D_{5/2}$ level.

In order to obtain an excitation spectrum, the 729 nm laser is tuned over the quadrupole transition in steps of about 1 kHz, and for any given laser detuning Δ the sequence (i)-(iii) is repeated 100 times to determine the excitation probability.

2.2 Results

2.2.1 Temporal variation of cavity field

In a first experiment we placed the ion close to a node of the SW field [12] and probed its response to the temporal variation of the intracavity field. The sign of the voltage ramp applied to the scan PZT determines whether the scan mirror moves towards the offset mirror or away from it. For a negative (positive) scan rate, i.e. mirrors moving towards each other (apart), the intracavity field is Doppler blue (red) shifted and thus the excitation spectrum will be red (blue) shifted, as the excitation laser detuning has to compensate for the Doppler shift. Fig. 8 shows a result where the cavity scan rate was one HWHM bandwidth in 6 lifetimes. The excitation spectra show the expected blue shift (red shift) for increasing positive (negative) scan rates. The peak excitation probability of more than 0.5 clearly demonstrates that the ion is coherently interacting with the intracavity field.

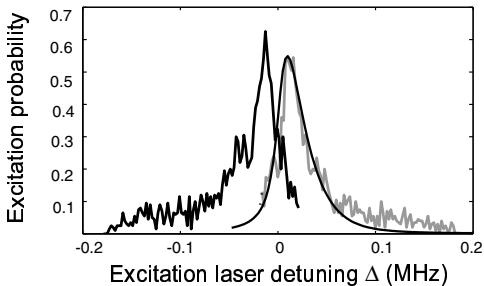


Figure 8: Excitation spectrum of the $S_{1/2} - D_{5/2}$ transition. The blue shifted excitation spectrum is drawn in gray on the right hand side of the diagram. The superimposed solid line shows the theoretical simulation with parameters: excitation laser bandwidth $\Delta\nu_{Laser} = 6$ kHz, maximum Rabi frequency at the transition center wavelength $\Omega_{max} = 15.5$ kHz.

We model the excitation for different laser detunings Δ by numerically integrating 2-level Bloch-equations using the time-dependent intracavity field calculated from the pertaining differential equations [13, 14]. The results of the simulation for positive scan rate is shown superimposed on the blue shifted spectrum in Fig. 8.

2.2.2 Spatial variation of cavity field

The second type of experiment probes the ion's response to spatial field variations. For this, we leave the scan rate at approximately the same value as in Fig. 8. The intensity of the 729 nm laser is adjusted such that the excitation is kept well below saturation. The offset voltage of both scan PZT and offset PZT is then varied simultaneously in

such a way that the SW in the cavity is shifted longitudinally with respect to the location of the ion. Fig. 9 displays the position-dependent excitation probability as function of the PZT offset voltage.

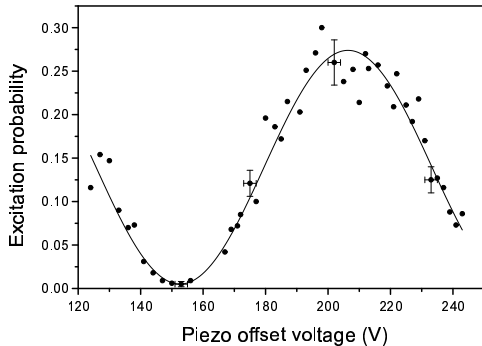


Figure 9: Excitation probability on the $S_{1/2} - D_{5/2}$ transition as function of the PZT offset voltage, i.e. at various positions in the intracavity standing wave field. The solid line represents a \sin^2 function fitted to the data points. Error bars given for representative data points are due to PZT hysteresis (abscissa) and the errors of the fit (ordinate).

The excitation probability varies spatially with the intensity of the SW [12]. A theoretical Bloch-equation analysis, as described above, predicts a nearly pure \sin^2 spatial variation, deviating by less than 1%. From a \sin^2 fit to the data points we obtain $V = 96.3 \pm 2.6\%$ contrast ratio (visibility V) in the position-dependent excitation. This very high visibility results from the strong confinement of the ion's wavefunction. The laser-cooled ion, oscillating with its secular frequencies and with thermally distributed amplitudes, has an rms spatial extension along the cavity axis of a_c , which leads to a reduction of the excitation contrast by a factor $\exp(-2(2\pi a_c/\lambda)^2)$. From the measured visibility V we find $a_c = 16_{-7}^{+5}$ nm. This small value of the spatial extension shows that in this experiment we cool the ion close to the Doppler limit (13 nm).

A necessary condition for all experiments relying on ion-cavity mode coupling is the ability to place the ion at a certain position of the intracavity SW field with high precision and high reproducibility [15]. In our experiment, the precision of positioning the center of the ion's wavefunction, using a measurement as in Fig. 9, is limited by the uncertainty in the measured excitation probability. From the error bars in Fig. 9 we deduce a spatial precision between 7 nm ($\approx \lambda/100$) at the position of largest slope and 12 nm and 36 nm at minimum or maximum excitation, respectively. We note, however, that the precision can be enhanced by averaging over a larger number of state detection measurements.

2.2.3 Coupling the quantum motion to the cavity field

Many schemes for quantum information processing with trapped ions rely on coherent interaction not only with the internal state but also with the motional degrees of freedom. A controlled coupling to the motional quantum state is a precondition for realizing such schemes. We recorded excitation probabilities of the ion at a fixed cavity scan rate (slightly larger than before), for different positions within the SW, and with the laser at 729 nm now tuned to either the carrier or the red axial sideband of the $S_{1/2} - D_{5/2}$ transition.

As displayed in Fig. 10, carrier and sideband excitations both map the SW spatial

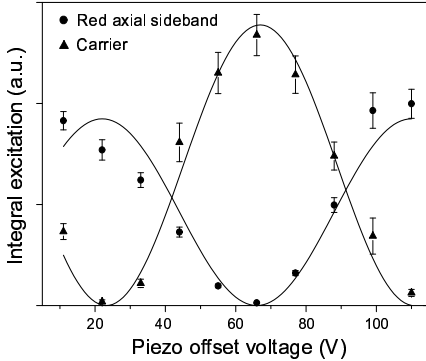


Figure 10: Excitation on the carrier (triangles) and the red axial sideband (circles) of the $S_{1/2} - D_{5/2}$ transition as function of the PZT offset voltage, i.e. at various positions in the intracavity standing wave field. The solid lines represent fits of \sin^2 functions to the data points.

field variation, but the traces are shifted by a phase factor of π . This phase shift arises due to symmetry characteristics of the transition matrix elements of carrier and sideband transitions in a SW field [16, 17]. Transitions changing the phonon number by even or odd integers are excited differently at different positions in the SW. The red sideband transition ($\Delta n = -1$) couples maximally at anti-nodes of the SW, whereas the carrier transition ($\Delta n = 0$) couples maximally at nodes.

The high-contrast orthogonal coupling of carrier and sideband transitions to the cavity mode enables applications such as cavity-assisted cooling [16] and entangling motional and photonic states when coupling to the cavity vacuum field [18, 19]. In particular, cavity-assisted cooling in a SW field means that sideband-cooling [10] on a red detuned vibrational sideband is facilitated by suppression of off-resonant carrier transitions which induce motional heating. In a similar fashion, unwanted off-resonant carrier excitations are suppressed when a cavity is used to drive sideband transitions in the Cirac-Zoller quantum-computing scheme [1]. This is interesting for applications since off-resonant carrier excitations impose a limit on the attainable gate speed [20].

3 Conclusions

Quantum information processing with trapped Ca^+ ions is investigated. High-contrast Rabi oscillations on carrier and sideband transitions are demonstrated as basic qubit manipulations. Procedures for measuring and compensating the ac-Stark shifts introduced by the manipulating laser were studied. Such a compensation is a necessary requirement for reliable quantum information processing. The application of composite pulses confines the operations to the computational subspace and was demonstrated with a composite phase gate operation.

In a second experiment the coupling of a high-finesse optical cavity mode to a narrow "qubit" transition in a single ion is studied. We find coherent cavity-ion interaction when the cavity mode is excited with resonant light. We also showed that by placing the ion into either nodes or anti-nodes of the standing wave in the cavity we can deterministically couple the cavity mode to the quantum motion of the ion. Future experiments might extend the current configuration towards trapping of two or more ions coupled to a common cavity mode, thus allowing for implementation of quantum logical gate operations.

Acknowledgements

We thank Ignacio Cirac and Peter Zoller for stimulating discussions and helpful comments. We gratefully acknowledge support by the European Commission (QSTRUCT and QI networks, ERB-FMRX-CT96-0077 and -0087, QUEST network, HPRN-CT-2000-00121, QUBITS network, IST-1999-13021), by the Austrian Science Fund (FWF, projects P11467-PHY and SFB15), and by the Institut für Quanteninformaton GmbH.

References

- † Permanent address: The MIT Media Laboratory, 77 Massachusetts Avenue, Cambridge, MA 02139-4307 USA.
- [1] J. I. Cirac, P. Zoller, Phys. Rev. Lett. **74** 4091-4094 (1995).
 - [2] H.C. Nägerl, Ch. Roos, D. Leibfried, H. Rohde, G. Thalhammer, J. Eschner, F. Schmidt-Kaler, and R. Blatt, Phys. Rev. A **61**, 023405 (2000).
 - [3] S. Stenholm, Rev. Mod. Phys. **58**, 699 (1986).
 - [4] C. Roos, T. Zeiger, H. Rohde, H. C. Nägerl, J. Eschner, D. Leibfried, F. Schmidt-Kaler, R. Blatt, Phys. Rev. Lett. **83**, 4713 (1999).
 - [5] H. C. Nägerl, D. Leibfried, H. Rohde, G. Thalhammer, J. Eschner, F. Schmidt-Kaler, and R. Blatt, Phys. Rev. A **60**, 145 (1999).
 - [6] A. M. Childs, I. L. Chuang, Phys. Rev. A **63**, 012306 (2001).
 - [7] M. H. Levitt, Prog. Nucl. Mag. Reson. Spectrosc. **18**, 61 (1986).
 - [8] H. Häffner *et al.*, to be published.
 - [9] J. I. Cirac, P. Zoller, H. J. Kimble, and H. Mabuchi, Phys. Rev. Lett. **78**, 3221 (1997).
 - [10] Ch. Roos, Th. Zeiger, H. Rohde, H. C. Nägerl, J. Eschner, D. Leibfried, F. Schmidt-Kaler, R. Blatt, Phys. Rev. Lett. **83**, 4713-4716 (1999).
 - [11] A. B. Mundt, A. Kreuter, C. Becher, D. Leibfried, J. Eschner, F. Schmidt-Kaler, R. Blatt, Phys. Rev. Lett. **89**, 103001 (2002).
 - [12] Note that the atomic quadrupole moment couples to the gradient of the electric field. The maximum excitation thus occurs at the nodes of the standing wave.
 - [13] H. Rohde, J. Eschner, F. Schmidt-Kaler, R. Blatt, J. Opt. Soc. Am. B **19**, 1425-1429 (2002).
 - [14] M.J. Lawrence, B. Willke, M.E. Husman, E.K. Gustafson, and R.L. Byer, J. Opt. Soc. Am. B **16**, 523 (1999).
 - [15] G. R. Guthöhrlein, M. Keller, W. Lange, H. Walther, K. Hayasaka, Nature **414**, 49-51 (2001).
 - [16] J.I. Cirac, R. Blatt, P. Zoller, and W.D. Phillips, Phys. Rev. A **46**, 2668 (1992).
 - [17] M. Šašura and V. Bužek, J. Mod. Opt. **49**, 1593-1647 (2002).
 - [18] V. Bužek, G. Drobný, M.S. Kim, G. Adam, and P.L. Knight, Phys. Rev. A **56**, 2352 (1997).
 - [19] F.L. Semião, A. Vidiella-Barranco, and J.A. Roversi, Phys. Rev. A **64**, 024305 (2001).
 - [20] A. Steane, C. F. Roos, D. Stevens, A. Mundt, D. Leibfried, F. Schmidt-Kaler, R. Blatt, Phys. Rev. A **62**, 042305 (2000).